Regional Multiseverity Casualty Estimation Due to Building Damage Following a Mw 8.8 Earthquake Scenario in Lima, Peru

Luis Ceferino,[a] Anne Kiremidjian,[a] and Gregory Deierlein[a]

This paper presents the application of a rigorous probabilistic framework that estimates the number, severity, and distribution of casualties over a region. A brief summary of the model is included in this paper. The application is for casualties resulting from a Mw 8.8 earthquake scenario occurring on the subduction fault along the coastline of Lima, Peru. The case study demonstrates an application of the casualty model, including the procedures for acquiring the required information, the selection of model parameters, and a step-by-step explanation of the model-solving algorithms. The model provides an estimate of the joint probability distribution of multiseverity casualties, including spatial and across-severity correlations. This paper also shows how the model can be useful for (1) estimating 90th-percentile casualties, (2) identifying unsafe communities and structural typologies, and (3) providing evidence to support hospital collaboration policies across different districts to increase the patient treatment reliability. Additionally, the results demonstrate that empirical fatality prediction methodologies can underestimate fatality rates in countries with scarce and outdated fatality data. [DOI: 10.1193/080617EQS154M]

INTRODUCTION

Casualties resulting from large earthquakes have resulted in heavy demands for health services on hospitals in many countries around the world. These demands can reach to tens (or even hundreds) of thousands (e.g., Turkey in 1999, China in 2008, Haiti in 2010; U.S. Geological Survey [USGS] 2015). Risk mitigation policies can reduce the number of casualties by decreasing buildings' vulnerabilities, and emergency planning can make the treatment of injuries more efficient and successful by improving the hospital functionality or enhancing the patient transportation capacities. Both risk mitigation and emergency planning measures to reduce earthquake injuries and fatalities can be informed by earthquake scenario studies that evaluate the casualty risk. The predictive studies can quantify statistics on the expected number of casualties, identify vulnerable infrastructure and communities, and explore the benefits of implementing emergency plans and mitigation policies.

This paper presents a predictive study of multiseverity earthquake casualties in Lima, Peru. The city is subjected to a Mw 8.8 earthquake scenario occurring at nighttime on the subduction zone off the coast of Peru. A probabilistic casualty model, developed previously by the authors (Ceferino et al. 2018), is implemented step by step. Two alternative

[a] John A. Blume Earthquake Earthquake Engineering Center, Department of Civil Engineering, Stanford University, 439 Panama Mall, Stanford, CA 94305; Email: ceferino@stanford.edu (LC, corr. author)

Earthquake Spectra, Volume 34, No. 4, pages 1739–1761, November 2018;

algorithms to solve the model are described herein. A brief summary of the casualty estimation model is included in this paper for completeness.

Key results of this study include the following: (1) estimation of casualties with varying severities, including confidence intervals, to assess post earthquake demands for hospital emergency services; (2) identification of the most vulnerable districts and building structural typologies in the city (i.e., with highest casualty rate); and (3) demonstration of how a collaborative hospital system response across districts improves the treatment reliability compared with a noncollaborative response (i.e., each district only treats casualties within corresponding jurisdictions). The study also shows that fatality rates obtained from Prompt Assessment of Global Earthquakes for Response (PAGER, Jaiswal et al. 2009) in countries without recent earthquake casualty data, or with fast-changing urban infrastructure, may be underestimated significantly.

The paper begins with a brief outline of the probabilistic casualty model and the two numerical algorithms proposed to solve the casualty model. Next, the paper describes the application, including the sources of information, the parameters of the probabilistic modules of the model, and the step-by-step analysis procedure for both algorithms. Finally, the resulting casualty estimates, as well as a discussion of their usefulness for policy making and emergency planning, are presented.

BRIEF DESCRIPTION OF THE MULTISEVERITY CASUALTY FRAMEWORK

Ceferino et al. (2018) presented a summary of earthquake epidemiology and proposed a probabilistic formulation for modeling of multiseverity casualties caused by earthquake damage over the affected region. Previous earthquake epidemiology studies reported that earthquake casualties, injury types, and injury severities depend on the complex interaction of the following: earthquake magnitude and location, the type and vulnerability of buildings' structural and nonstructural components, building uses and occupancy levels at the earthquake occurrence time, age and gender of individuals, and individuals' actions during the earthquake (Goncharov and Frolova 2011, Johnston et al. 2014). Most, though not all, of these components were included in the formulation presented by Ceferino et al. (2018) and applied in this study. The probabilistic formulation is divided into the following three modules:

1. The Ground Motion Intensity module estimates peak ground accelerations (PGAs) and spectral accelerations [Sa(T)] over the region of interest. Ground motion prediction equations (GMPEs, e.g., Zhao et al. 2006) along with models that account for between- and within-event correlations across vibration periods and building locations (e.g., Goda and Atkinson 2009, Markhvida et al. 2018, respectively) are required as input of the module. Additionally, this module requires information on the Earthquake Event and the Soil Condition information, where:
    - The Earthquake Event information defines the earthquake scenario that will be analyzed, including the earthquake magnitude, the earthquake rupture dimensions, and its location along the seismic fault.
    - The Soil Condition information consists of the values of shear wave velocities of the top 30 m (V_{S30}) of the sites in the region of interest.

2. The Building Damage module estimates the damage in the buildings affected by the ground shaking. Parameters that define relationships between ground motion and damage probability are required for each structural typology. This module requires the Building Structural Typology information, which includes the identification (or estimation) of the structural typologies of all buildings and their locations.
3. The Population Health State module estimates the casualties (i.e., multiseverity injuries and fatalities) caused by damaged infrastructure (from the Building Damage module). Parameters that define the probability of occupants' injury severity for the given building damage are required for each structural typology. This module requires Building Occupancy Dynamics information, which defines the occupancy of each building in the region according to the time of the earthquake occurrence (e.g., during commuting hours, the working day, or nighttime).

NUMERICAL EVALUATION DESCRIPTION

The objective is to estimate the joint distribution of the multiseverity casualties over a region defined by a vector $\boldsymbol{I_T}$ that contains N_{HS} elements. Each element in $\boldsymbol{I_T}$ represents the number of population with a different casualty severity. The probability distribution of $\boldsymbol{I_T}$ cannot be solved in closed form because of the complexity of the probabilistic models. When the number of buildings in the study region is small, interpolation or quadrature-based methods can be applied. For a large number of buildings, these methods are not able to solve the problem. In such cases, the following two numerical algorithms have been shown to work well in Ceferino et al. (2018) to solve the casualty estimation.

ALGORITHM 1: FORWARD MONTE CARLO

The first algorithm is based on forward Monte Carlo simulation. As shown in Figure 1a, $N_{\text{real.}}$ realizations of health states $\boldsymbol{I_T}$ are sampled, which are then used to calculate the mean and variances of casualties for different casualty severities, correlations among different health states, or, more generally, the joint probability distribution of $\boldsymbol{I_T}$. Each sample of $\boldsymbol{I_T}$ is estimated by first sampling the earthquake ground motion intensities (in the Ground Motion Intensity module) and then sampling the building damage states (in the Building Damage module) and corresponding casualties (in the Population Health State module). Each sample of $\boldsymbol{I_T}$ is estimated by aggregating all casualties occurring in the region.

To estimate spatial correlations of health states across different communities, the algorithm is modified as follows (see Ceferino et al. 2018 for details). For each casualty realization, m, two aggregated casualty vectors are found, $\boldsymbol{I_{T1}}$ and $\boldsymbol{I_{T2}}$, each of which corresponds to a different community of the city. They are calculated as the sum of casualty vectors in buildings over their corresponding geographical regions. Then, using these sets of samples, the covariance (and correlations) between $\boldsymbol{I_{T1}}$ and $\boldsymbol{I_{T2}}$ are estimated. It should be noted that the city can be subdivided into more than two communities, and correlations of health states between any pair of communities can be found through the same process.

ALGORITHM 2: MONTE CARLO AND CENTRAL LIMIT THEOREM

The second algorithm is based on a combination of Monte Carlo analysis and the Central Limit Theorem (CLT). Figure 1b shows a flow diagram of this algorithm. When the number

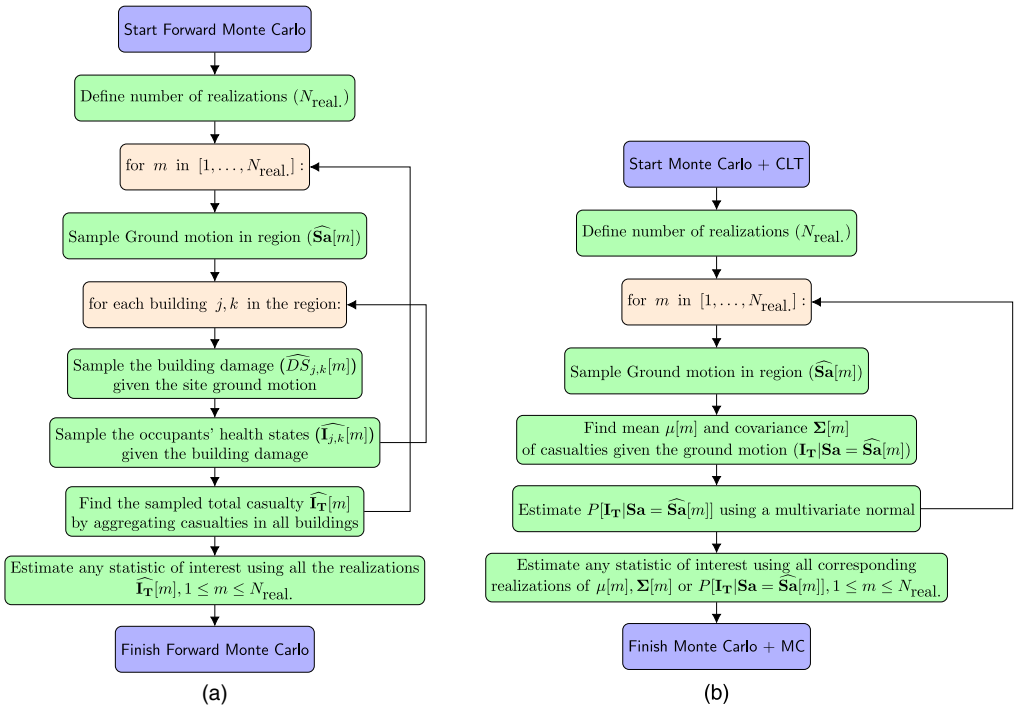

Figure 1. Flow diagram of two algorithms of the model: (a) Algorithm 1; and (b) algorithm 2.

of casualties is large, the joint probability distribution of $\boldsymbol{I_T}$ can be estimated based on CLT. Previously, Ceferino et al. (2018) proved the validity of this algorithm for cases where the mean number of casualties is larger than 100 (i.e., errors lower than 2×10^{-2} in the CDF estimate of casualties conditioned on ground motion). This algorithm gave valid results for cases with even lower numbers of casualties, but either a special individual inspection or statistical testing (e.g., two-sample Kolmogorov–Smirnov test) were needed to support the validity of the results. The probability $P[\boldsymbol{I_T}]$ can be estimated by averaging all the $N_{\text{real.}}$ of $P[\boldsymbol{I_T} \mid \boldsymbol{Sa}]$. Other statistics of interest can be calculated without any requirement on the number of casualties, for example, mean and variances of casualties for different severities, correlations among different health states, and spatial correlations of health states across different communities. As seen in Figure 1b, in this algorithm, the Building Damage module, the Population Health State module, and the aggregation of casualties over the region are coalesced, and the casualty vector, $\boldsymbol{I_T}$, conditioned on the ground motion intensity, is represented as a multivariate normal distribution. This makes the algorithm significantly faster than Algorithm 1.

To estimate spatial correlations of health states across different communities, Algorithm 2 is slightly modified. For each casualty realization m, the covariance matrix $\mathbf{\Sigma}_{(\boldsymbol{I_{T1}},\boldsymbol{I_{T2}} \mid \boldsymbol{Sa})}$ between health states of two communities for a given ground motion realization can be

readily found (see Ceferino et al. 2018 for details). Using the covariance realizations, the final covariance (and correlations) between $\boldsymbol{I_{T1}}$ and $\boldsymbol{I_{T2}}$ can be estimated. Similar to Algorithm 1, a large region can be subdivided into more than two communities, and correlation of health states between any pair of communities can be found through the same process.

CASUALTY MODEL APPLICATION

This section demonstrates an application of the formulation by assessing the casualty occurrences for a large earthquake scenario in Lima, Peru. Here, the following is shown: (1) the sources of information and the parameter selection for the probabilistic modules; (2) a step-by-step explanation of the sampling process of Algorithms 1 and 2; (3) the variety of results and information that are obtained, including the identification of communities and structural typologies that are the most susceptible to damage in an earthquake, the correlations between casualty severities, and the spatial correlation of casualties across communities; and (4) a demonstration of how this methodology can provide evidence for supporting a collaborative hospital response across communities rather than an individual, within-community response.

CASE STUDY DESCRIPTION

The model is applied to an earthquake scenario of magnitude 8.8 that is assumed to occur at night. This is to represent the earthquake that occurred in 1746 at the subduction zone along the coast of Lima (Beck and Nishenko 1990), which is the largest known event to have affected Lima. Over the past few decades, the population of Lima has grown significantly, with a current population of almost 10 million people. The fast population growth spurred massive new housing developments built with no engineering expertise or proper design. As the last big earthquake (Mw 8.0) occurred in 1974, most of the new infrastructure has not experienced a major seismic event. Therefore, this scenario study can be relevant for disaster mitigation planning in the city. The earthquake rupture dimensions and location are shown in Figure 2a, and the spatial distribution of people affected by the earthquake is shown in Figure 2b. The following sections include details of (1) the information sources and parameters of the probabilistic models and (2) the step-by-step procedure of Algorithms 1 and 2 for the case study.

Information Sources and Model Parameters

1. Ground Motion Intensity module: The distribution of ground motion intensities in the study region was assessed by coupling the contributions of median ground motions and between- and within-event correlation of ground motion residuals. The GMPE proposed by Zhao et al. (2006) was used to estimate the median ground motions and the within- and between-event variances. OpenQuake software (Silva et al. 2014) was used to estimate the median ground motion values across the region at 1×1 km grid points. The within-event residuals are estimated using the methodology proposed by Markhvida et al. (2018), and the between-event residuals are estimated using the model proposed by Goda and Atkinson (2009).
    - Earthquake Event information: The rupture studied here is a Mw 8.8 event in the subduction zone that replicates the 1746 Lima earthquake (Beck and Nishenko 1990) based on the rupture location estimated by Dorbath et al. (1990).

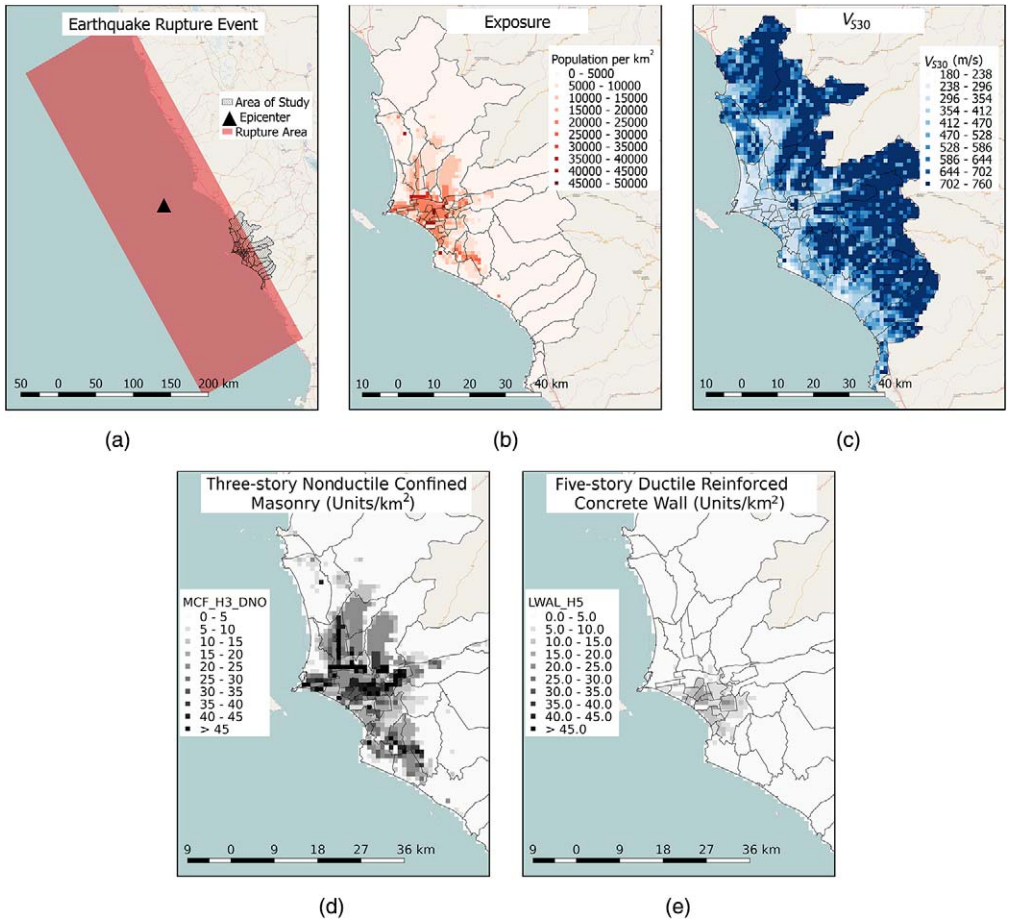

Figure 2. Different information sources of the model. (a) Earthquake rupture; (b) distribution of population; (c) shear wave velocity (m/s); (d) three-story nonductile confined masonry; and (e) five-story ductile concrete wall.

The rupture dimensions were estimated using scaling relationships proposed by Wells and Coppersmith (1994). The red rectangle shown in Figure 2a represents the ruptured area, where the dashed areas show the extent of Lima city. The geographical information system (GIS) files containing the geometry and location of the rupture are provided in the online Appendix.

- Soil Condition information: V_{S30} values, shown in Figure 2c, were inferred from existing microzonation maps for Lima (i.e., Aguilar et al. 2013) based on soil types recommended in Ministerio de Vivienda (2016). Where microzonation information was not available, V_{S30} was estimated from the slope of the terrain using the equation proposed by Allen and Wald (2007). The V_{S30} map is provided in the online Appendix.

2. Building Damage module: Fragility functions developed for South American buildings were used for estimating the building damage (Villar-Vega et al. 2017). The fragility function set has detailed categories of structural typology, varying according to the structural system, number of stories, and ductility properties. In total, 36 structural typologies were considered. The list of structural typologies is provided in the online Appendix, along with the intensity measure inputs of the fragility function for each typology. The 36 categories use either PGA, Sa(0.3), or Sa(1.0), all of which are modeled in the Ground Motion Intensity module. A set of six damage states were considered: ds_1 – None; and ds_2 – Slight; ds_3 – Moderate; ds_4 – Extensive; ds_5 – Complete without structural collapse; ds_6 – Complete with structural collapse. Villar-Vega et al. (2017) provides fragility functions for the first five damage states but not for "structural collapse" (ds_6). The fragility function for (ds_6) was found as the product of the fragility function for complete damage (ds_5) and a rate for structural collapse provided in HAZUS (Federal Emergency Management Agency [FEMA] 2015). These rates were extracted from HAZUS's structural typologies. The online Appendix also provides the assumed equivalences between HAZUS and the typologies used in this application. Figure 3a and 3b show the fragility functions for three-story nonductile confined masonry and five-story ductile reinforced concrete wall buildings, respectively. It can be seen that the nonductile confined masonry structures, which are assumed to have been built without seismic design considerations, are considerably more vulnerable than the ductile reinforced concrete wall buildings, which are assumed to be built following modern seismic design requirements.

    - Building Structural Typology Information: The number of buildings corresponding to each typology was obtained at a district level from existing studies (GEM Secretariat 2015, Yepes-Estrada et al. 2017). In order to obtain a finer resolution of building spatial distribution, the buildings of each typology were redistributed within the districts according to the population spatial distribution. The redistribution was directly proportional to the number of people in a spatial grid of population per square kilometer. The grid was obtained from LandScan (Oak Ridge National Laboratory 2013), and it represents the 24-hour average number of people occupying each square kilometer. The final spatial distribution of building typologies is provided in the online Appendix in GIS format. Figure 2d and 2e show the estimated spatial distributions of three-story nonductile confined masonry and five-story ductile reinforced concrete wall buildings. The graph indicates that there are fewer five-story ductile reinforced concrete wall buildings than three-story nonductile confined masonry buildings. Additionally, the former are located mostly in the center of the city, whereas the latter are located on the peripheries of the city; this exemplifies that the more vulnerable buildings (see Figure 3a) are mostly in the periphery.

3. Population Health State module: The following five health state categories proposed by HAZUS were adopted: hs_1 – Noninjured; hs_2 – Severity 1; hs_3 – Severity 2; hs_4 – Severity 3; and hs_5 – Fatality. Casualty Severity 1 represents the individuals whose treatment does not require hospitalization; Casualty Severity 2 represents individuals

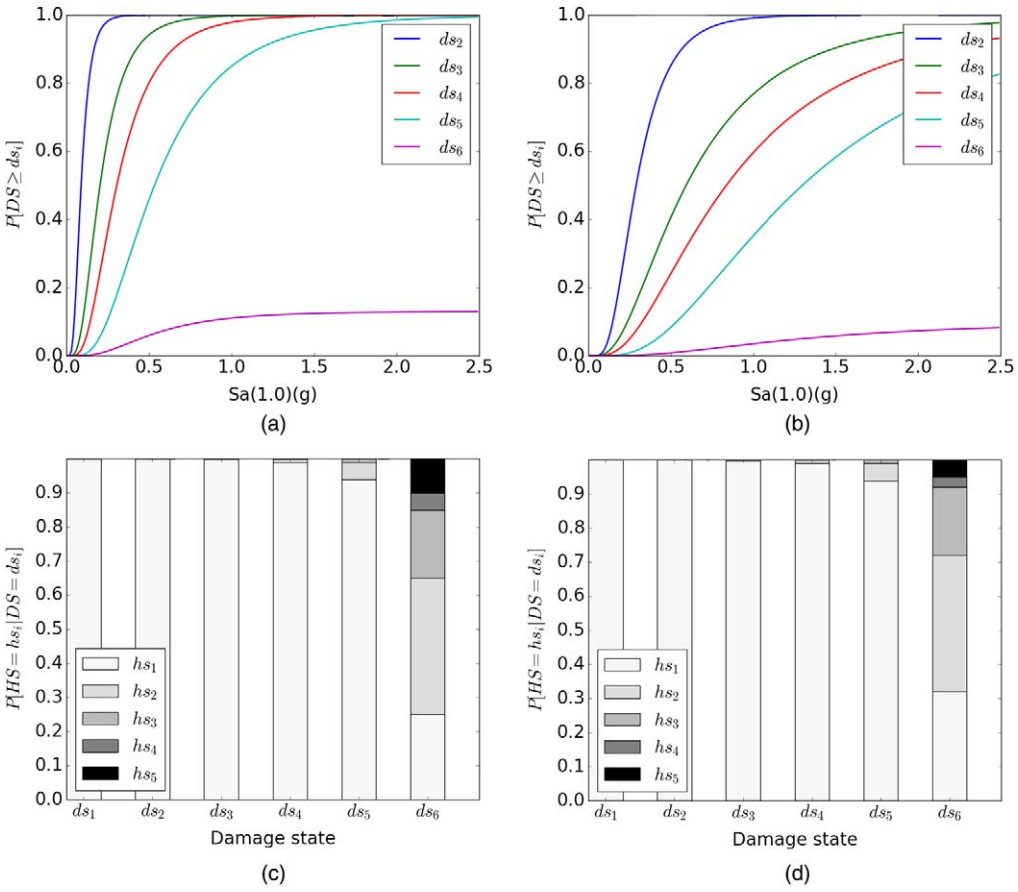

Figure 3. Fragility functions: (a) Three-story non-ductile confined masonry; and (b) five-story ductile concrete wall. Probabilities of occupant casualty occurrence: (c) Three-story non-ductile confined masonry; and (d) one-story light wood.

whose treatment requires hospitalization, but the injuries are not life-threatening in the short term; and Casualty Severity 3 represents individuals whose treatment requires immediate hospitalization, as their injuries are life-threatening in the short term. Rates of casualties conditional on damage states from HAZUS are used herein (FEMA 2015), where the rates vary according to structural typology. These rates are used as marginal probabilities that an occupant has a certain health state given the building damage state. The probability of not being injured was calculated so that the sum of all possible health states adds to one. Because the structural typologies of HAZUS are not identical to the typologies used in this application, the HAZUS rates were mapped to the typologies used in this case study. This mapping is the same as the one used for collapse rates in the Building Damage module and is shown in the online Appendix. The typologies were chosen in terms of similar construction material, building weight and height, and structural

system so that the probability of occupant casualty given damage is similar. The casualty rates can be found in *FEMA* (2015). Figure 3c shows a stacked bar chart of these probabilities for each of the damage states of three-story nonductile confined masonry buildings. It can be seen that for nondamage, slight, and moderate damage (ds_1, ds_2, ds_3), the probability of any casualty is either zero or very low. For extensive and complete damage without collapse (ds_4, ds_5), the probability of being injured with severity 1 starts to be significant. For collapse (ds_6), the probabilities of being injured increase, and the probability of fatality is significant (10%). In general, lighter structures have smaller casualty probabilities than heavier ones. This is exemplified in Figure 3d, which shows the relatively low casualty probabilities for one-story light wood buildings. It is known that the HAZUS casualty rates were obtained using expert opinion within the United States context. Though data on casualty rates are scarce, the fatality rates from HAZUS were verified to closely match fatality rates in collapsed buildings found in developing countries. The fatality rate estimated from the data collected in the 2005 Pakistan earthquake (Noh et al. 2017) was 10.7%, which is close to the rates (10%) of most of the building typologies in HAZUS. Therefore, these data support the use of the HAZUS casualty rates in the case study for Lima.

- Occupancy Dynamics Information: The occupancy of buildings was estimated from the LandScan information (Oak Ridge National Laboratory 2013). Figure 2b shows the population per square kilometer as obtained from LandScan and distributed to each building proportionally to the buildings' number of stories and estimated footprint areas. It was assumed that all people were within the assigned building for the nighttime occupancy. The relative gross areas per each typology and the estimated spatial distribution of building occupants are provided in the online Appendix. While this case study considered only the nighttime occupancy, other occupancies (e.g., during the working day or commuting hours) would need to be evaluated for a more complete assessment of the casualty risk.

Flow of Analysis in Algorithms 1 and 2

The two algorithms presented previously were used to estimate the joint distribution of the multiseverity casualty occurrence. The following paragraphs describe the step-by-step procedures for applying the two algorithms:

1. Ground Motion Intensity module: The ground motion intensities, PGA, Sa(0.3s), and Sa(1.0s) are sampled at the respective building locations according to their fragility function input requirements. First, the median intensity values are estimated using the Earthquake Event information, the Soil Condition information, and the GMPE (Zhao et al. 2006). Realizations of these intensities are then estimated by calculating within-event and between-event residuals according to the models proposed by Markhvida et al. (2018) and Goda and Hong (2008), respectively. Results of this step are shown in Figure 4a and 4b, which show one realization of PGA and Sa(0.3s) over the region. Each of the graphs shows that the regions with high (or low) ground motions are clustered in space, revealing the spatial correlation

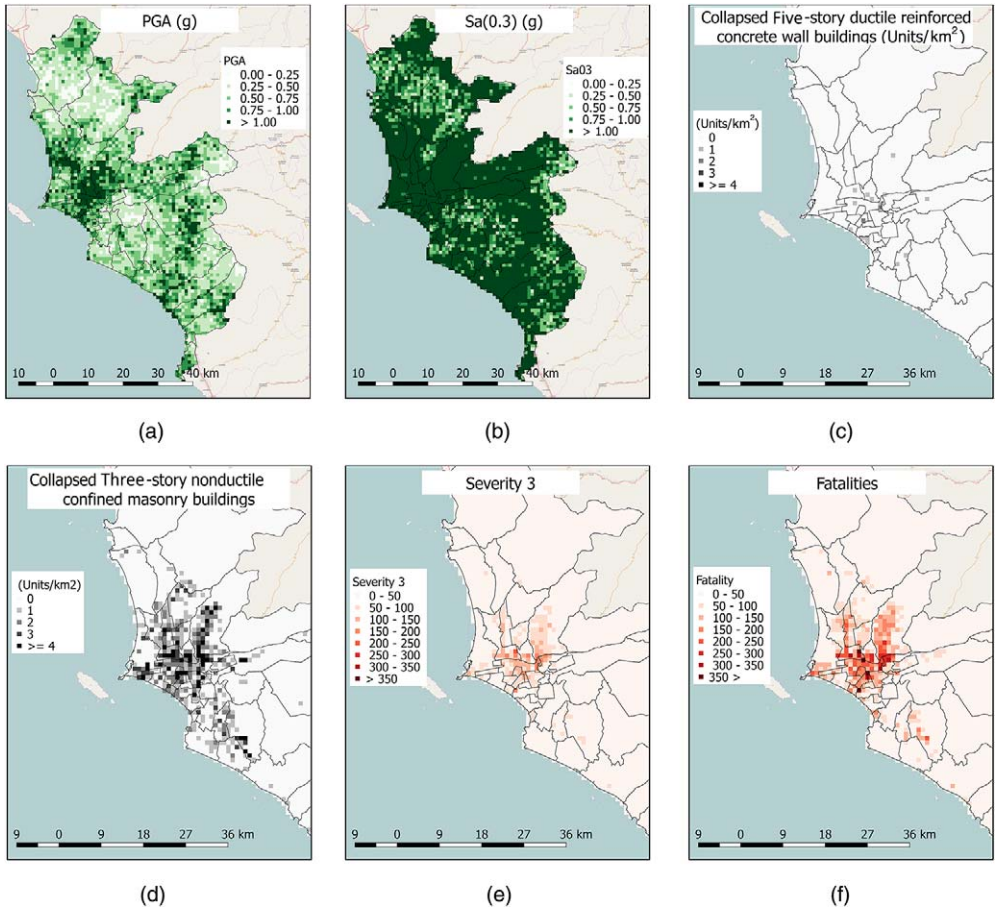

Figure 4. Results from algorithm 1. One realization of ground motion intensities: (a) PGA; and (b) Sa(0.3s). One realization of collapsed houses (units/km^2): (c) 5-story concrete wall; and (d) three-story confined masonry. One realization of casualties (per km^2): (e) severity 3; and (f) fatalities. Panels (a, c, f) are reprinted with permission from Ceferino et al. (2018).

of the model. Additionally, regions with high (or low) PGA and Sa(0.3s) values are the same, highlighting the close correlation between PGA and Sa(0.3s).

2. Building Damage module: Only Algorithm 1 samples the damage state conditioned on the ground motion intensities. Algorithm 2 skips this step. The damage state of each building, given the ground motion at the site, is sampled independently from other buildings. The probability of being in different states is calculated using the fragility functions for respective structural typologies. Figure 4c and 4d show one realization of five-story ductile reinforced concrete wall and three-story nonductile confined masonry buildings, respectively, that collapsed because of the ground motion realization shown in Figure 4a and 4b. As expected, there are fewer collapses of ductile reinforced concrete wall buildings. Correlation between the collapses

across these two different structural types is apparent owing to the correlation of the ground motion intensities.

3. Population Health State module: Only Algorithm 1 samples the occupants' health states conditioned on the building damage states. Algorithm 2 skips this step. The occupants' health states are independently sampled for each building according to the building damage. The probability of being at any health state is given for each structural typology for each possible damage state. Within each building, the health states of the occupants are sampled using a multinomial distribution with as many trials as number of occupants in the building. Figure 4e and 4f show the realization of the number of casualties with severity 3 and the fatalities, respectively. It can be seen that there is correlation over the space and across different health states. The number of people with severity 3 and casualties are high (or low) in roughly the same places, which demonstrates the correlation with building damage and collapses.
4. Aggregated casualties: To calculate the casualties over all the region, Algorithm 1 sums the casualties over the whole region for each of the health states. On the other hand, Algorithm 2, which skipped the sampling of damage states and casualty occurrence at each building, requires the calculation of the mean casualty vector and covariance casualty matrix given the ground motion intensity realization. Then, the probability of the aggregated health states' population is found using a multivariate normal distribution. Figure 5a and 5b show a comparison of the results of one sample resulting from Algorithms 1 and 2. The red dot in Figure 5a indicates the aggregated casualty realization for injuries with severity 3 in the x-axis and fatalities in the y-axis based on the sum of casualty realizations determined by Algorithm 1 and shown in Figure 4. The joint normal distribution of the total number of injured with severity 3 and fatalities resulting from Algorithm 2 are shown by the black contours. These contours were calculated using the same realization of the ground motion intensities shown in Figure 4a and 4b. The number of casualties with severity 3 are compared in Figure 5b, in which the realization from Algorithm 1 is shown with the red dashed line, and the distribution from Algorithm 2 is shown with the black bell curve.

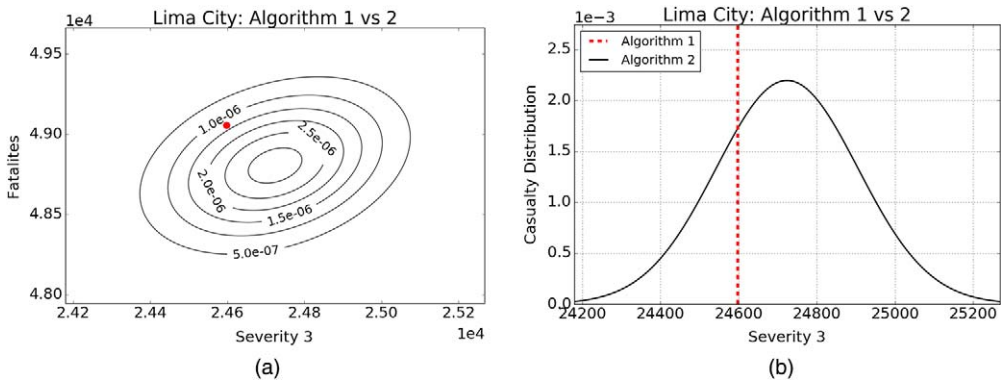

Figure 5. Comparison of Algorithms 1 and 2: (a) Severity 3 and fatality; and (b) severity 3.

This subsection has described the procedure for obtaining one realization of the multi-severity casualty model. The next subsections show the set of possible results that this methodology generates by using and combining many casualty realizations. In terms of efficiency, Algorithm 2 is faster than 1, but it only can be reliably used when there is a sufficiently large number of casualties. Other statistics (e.g., mean, variances, and correlations) can be found without any requirement on the number of casualties. For the whole Lima region, Algorithm 2 is as accurate as Algorithm 1, as shown in Ceferino et al. (2018).

ANALYSIS OF RESULTS

This subsection describes the results and information that can be extracted from the casualty analysis and the potential use of these results to support risk mitigation policy decision making.

Region-Wide

Multiple realizations of Algorithm 2 were combined to obtain the final distribution of casualties in Lima city. Figure 6a and 6b show the probability distribution of the total number of injured with severity 3 and fatalities, respectively. Note that the normal distributions from the sampling process of Algorithm 2 had to be discretized, as the number of casualties can only take non-negative integers. The graphs show that these final distributions are very skewed. Means and standard deviations for each health state are reported in Table 1, in which the coefficients of variation range from 70% to 80% (except for the noninjured health state). The fourth and fifth columns of Table 1 show the likelihood of the interval $[\mu - \sigma, \mu + \sigma]$ for each health state. The probabilities associated with these intervals are close to 0.70. The fourth column shows the 90th percentile for each of the health states (i.e., there is only a 10% chance to exceed these values). This percentile can be used as a target for

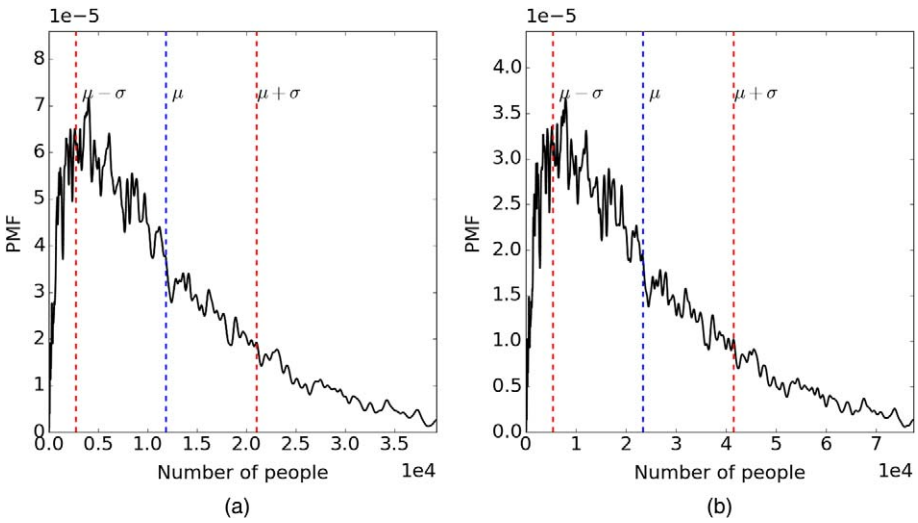

Figure 6. Distribution of casualties with different severities in Lima city: (a) Severity 3; and (b) fatalities.

Table 1. Summary of the aggregated multiseverity casualty estimations in Lima city

Health state	μ	σ	$[\mu-\sigma, \mu+\sigma]$	p	$I_{90\%}$	$\frac{I_{90\%}-\mu}{\sigma}$
Noninjured	8 789 648	251135	[8 538 513, 9 040 783]	0.70	9 064 258	1.09
Severity 1	234 290	169 105	[65 185, 403 395]	0.69	480 108	1.45
Severity 2	74 584	54 918	[19 666, 129 502]	0.70	154 132	1.45
Severity 3	11 856	9 121	[2735, 20977]	0.71	25 047	1.45
Fatality	23 405	18 017	[5388, 41422]	0.71	49 464	1.45

the community if they want to prepare to treat all the casualties with high confidence for the earthquake scenario. The fifth column shows the distance from $I_{90\%}$ to μ, normalized by σ. For all health states (except for noninjured health state), this normalized distance was 1.45. This suggests that in the absence of the probability distribution of casualties, $\mu + 1.45\sigma$ could be used to benchmark $I_{90\%}$.

The estimated number of fatalities and injuries with high severity is large, in which the mean number of fatalities is approximately 23,000 out of the 10 million people living in Lima. These results gives new insights into what may happen when the next Mw 8.8 earthquake strikes Lima. As a point of reference, the 1746 Mw 8.8 earthquake occurred at night and caused almost 1,500 fatalities when only 60,000 people lived in Lima (Walker 2008). The predicted casualties in Lima are comparable to the 1999 Mw 7.6 İzmit earthquake in Turkey, where approximately 17,000 people died (USGS 2015). The model estimated mean number of casualties with severity 3, 2, and 1 of roughly 12,000, 75,000, and 234,000, respectively. It is challenging to know whether these predicted demands on the hospital system are similar to the İzmit earthquake. The İzmit earthquake caused 44,000 injuries, but there is no information of the severity of these injuries or if these data are exhaustive (i.e., injuries are less likely to be reported than fatalities, especially low-severity injuries). Future studies will collect the required data to investigate the 2007 Mw 8.0 Pisco earthquake and use the model to reproduce the close to 500 fatalities that occurred as a result of the shaking.

Per District

The rates of casualty occurrence in each district are described here. These rates were found by dividing the expected number of casualties in each district by the number of people in the district. These expected values were calculated using Algorithm 2. Figure 7a shows these rates in each of the districts and the global rate in the entire city. The districts are shown in order of decreasing fatality rate, where the red bars represent the fatality rates, the blue bars represent the rates of casualties with severity 3, and the green bars represent the casualties with severity 2. The global rate was found by dividing the mean number of casualties in the whole Lima city (see Table 1) over the total population. These rates are drawn using dashed lines and the corresponding colors in Figure 7a. The districts with higher rates (i.e., the most unsafe) are the ones closer to the rupture (along the coast), such as Barranco, La Punta, La Perla, Villa El Salvador, and Callao. The districts in the periphery, such as Ate Vitarte and San Juan de Lurigancho, are known for having most of their buildings without proper engineering design; however, they do not rank at the top of the casualty rates. Located further from the coastline, these districts tended to experience lower ground motions. It seems,

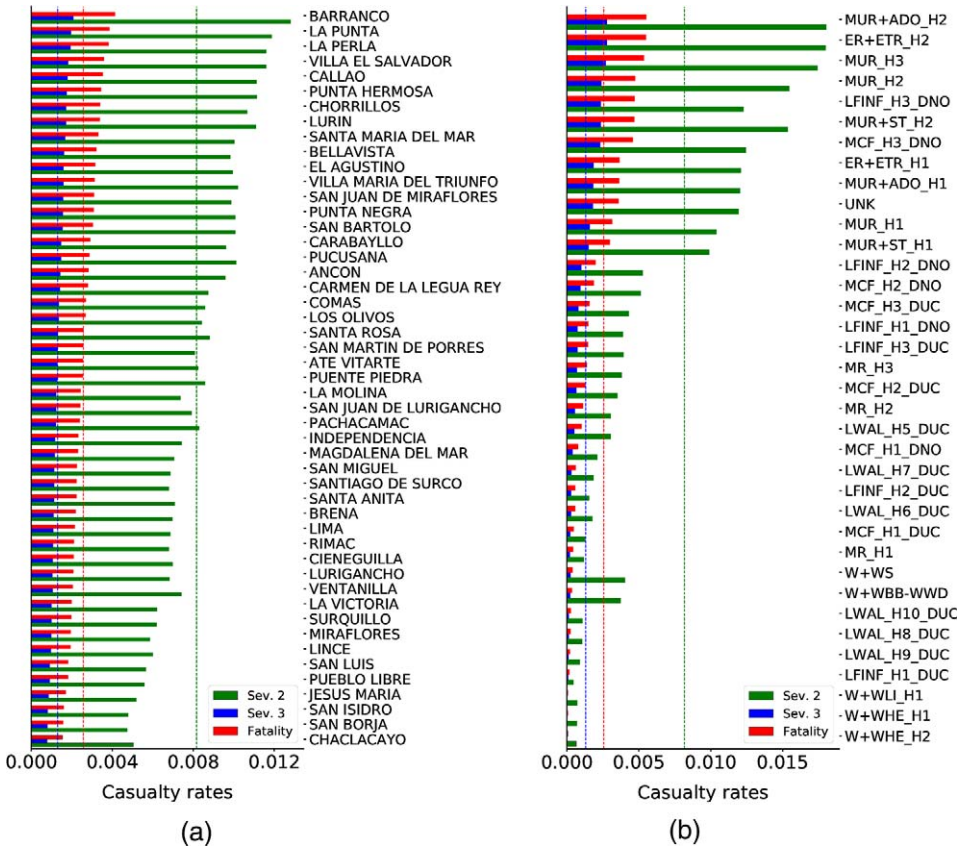

Figure 7. Rates of casualties: (a) In districts; and (b) in structural typologies. Fatalities in red, injured with severity 3 in blue, and injured with severity 2 in green. Dashed lines represent respective global rates in the whole Lima city.

therefore, that the large ground motions in the areas close to the rupture dominate the casualty occurrence in this application. There is a high variability among districts in the resulting rates. The lowest-rate district, Chaclacayo, has rates of fatality and casualty with severity 3 that are almost two times smaller than the highest rate district, Barranco.

Per Structural Typology

The rates of casualty occurrence corresponding to each structural typology are described here. The casualties rates for each structural typology were computed by dividing the sum of expected number of casualties within buildings with the same structural typology by the total number of occupants of these buildings. The expected values of the number of casualties within each building typology were found using Algorithm 2. Figure 7b shows these rates for each structural typology. The typology labels correspond to the 36 structural typologies in the city. They describe the structural system, the number of stories, and whether they are ductile structures. The complete descriptions of these typologies and their associated codes are provided in the online Appendix. The structural typologies are shown in

order of decreasing fatality rate. In Figure 7b, the red bars represent the fatality rates, the blue bars represent the rates of casualties with severity 3, and the green bars represent the casualties with severity 2. The dashed lines with corresponding colors show the global casualty rates in all the region. The graph shows that there is significant difference of the occupants' casualty likelihood according to the building structural typology. The results indicate that occupying a two-story adobe building increases the occupant fatality rate 20 times compared with a ten-story ductile reinforced concrete wall building. The most dangerous structural typologies (i.e., with highest casualties rates) are one- and two-story adobe and rammed earth, two- and three-story unreinforced masonry, and three-story nonductile confined masonry and nonductile concrete frames with infill. The wooden buildings are often constructed without proper seismic engineering design and with improper construction practices; however, the results show that their casualty rates are among the lowest. This is because the lightness of these structures makes them less vulnerable (less likely to collapse), and even if they collapse, they are less likely to injure the occupants than other heavy structures (e.g., masonry or concrete buildings).

Comparison with PAGER

In this subsection, the fatality rate estimated with the proposed model is compared with the country-specific fatality rates estimated by PAGER for different modified Mercalli intensities (MMI). The PAGER system uses quick estimations of MMI to predict fatalities immediately after an earthquake. PAGER estimates the relationship between MMI and fatality rates by performing regression analysis on previous country-specific earthquake fatality data. The fatality rate measures the expected number of fatalities over the number of affected population. Table 2 shows the comparison between PAGER fatality rates for Peru, Japan, and Turkey, and the fatality rate resulting from the proposed casualty model. The parameters of the PAGER fatality functions were obtained from Jaiswal et al. (2009) and Jaiswal and Wald (2010). The PAGER system combines the total population exposure estimated at MMI IX and X and refers to it as MMI IX+. The MMI IX+ fatality rate is calculated as the MMI IX rate, and MMI IX+ represents the maximum fatality rate in the PAGER analysis. It can be seen that the fatality rate estimated with this model is almost ten-times higher than the PAGER rates for MMI IX+. The fatality rate estimated with the model presented herein was calculated to be 2.6×10^{-3} fatalities per capita. The rate was estimated as the mean

Table 2. Comparison of fatality rates (i.e., number of earthquake fatalities per affected population) with PAGER

Casualty model (this paper)			
2.6×10^{-3}			
PAGER (MMI)			
Country	VII	VIII	IX+
Peru	3.3×10^{-5}	9.8×10^{-5}	2.4×10^{-4}
Japan	4.9×10^{-8}	3.2×10^{-5}	2.4×10^{-3}
Turkey	3.5×10^{-6}	8.0×10^{-4}	2.4×10^{-2}

number of earthquake fatalities over the total population in the analysis. The PAGER rate is 2.6×10^{-4} fatalities per capita for MMI IX+ for Peru.

As mentioned previously, PAGER performs a regression on country-specific data to estimate fatality rates. PAGER rates are assumed to be time stationary. The data from large earthquakes are combined without accounting for changes over time in the infrastructure inventory and the vulnerabilities. The infrastructure inventory and its vulnerability vary over time because of building seismic code improvement, the infrastructure's deterioration, or the incremental construction problem (Lallemant et al. 2017). Additionally, as large earthquakes are rare events, data are scarce, especially in locations where no large earthquakes have occurred in recent decades (i.e., locations with long seismic gap). For example, PAGER's fatality rates in Peru were estimated from 33 previous earthquakes, in which all of the fatalities were under 1,000 and only two out of the 33 earthquakes had fatalities exceeding 100 (Jaiswal et al. 2009). In contrast, data from Japan and Turkey include earthquakes with a larger number of fatalities in recent years; therefore, their estimated fatality rates are higher. The fatality rate for MMI IX+ in Japan is ten-times larger than the corresponding rate in Peru. This is a striking difference as Japan is characterized by less vulnerable infrastructure as a result of a more stringent seismic code with stricter enforcement than Peru. The last row in Table 2 shows PAGER's rates for Turkey. The rate for MMI IX+ in Turkey is 100-times larger than the one for Peru. This significant difference suggests that the fatality rate for Peru is underestimated because of the lack of recent earthquakes with a large number of fatalities. It should be noted, however, that the latest version of PAGER has a new version of fatality rates. While the Turkey and Japan rates have not been changed significantly, the Peru fatality rates have increased significantly. The new PAGER fatality rate for MII +IX in Peru is 1.1×10^{-3}, which is much closer to the fatality rate found in this study (2.6×10^{-3}). Further comments or conclusions cannot be drawn, as background and substantiating data for the recent PAGER updates have not been found in the literature.

In summary, the observations outlined in this subsection indicate that the model presented in this paper can result in significantly different fatality rate estimates from country-specific data-driven fatality models. The comparisons of the fatality rates among different countries suggest that data-driven models could underestimate fatalities in countries where earthquake fatality data are scarce and not recent. In countries where there have not been recent earthquakes, this proposed model can be a more reliable alternative as it incorporates more detailed information in the analysis, such as occupancy levels at the time of the earthquake and the current building exposure and vulnerabilities in the region of analysis.

Correlation Across Severities

The proposed model can also estimate the correlations among the different health states. The correlation analysis across health states is key (1) to understand the dependencies across casualty occurrence with multiple severities and (2) to provide the basis for analyzing the joint probability distribution of multiseverity casualty occurrence. These correlations and joint distributions can be important for policy decisions such as multiseverity injury treatment. Preevent planning can be more rational and effective if information on the number of casualties and their severities can be jointly predicted. Figure 8 shows the correlation matrix of the health states as a heat map for Lima city and one district, San Bartolo (Figure 8a and 8b, respectively). These correlation matrices were estimated using Algorithm 2. It can be seen that the

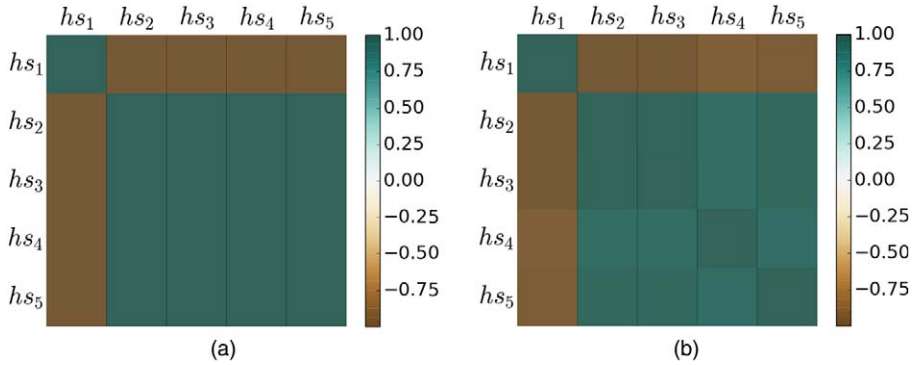

Figure 8. Correlation matrix (as heat map) of the number of people in different health states: (a) Lima city; and (b) San Bartolo district.

number of noninjured is negatively correlated with all the other health states. This is intuitively expected, as a high number of noninjured population implies that there are few casualties. All other health states are positively correlated among each other. In general, the model shows strong correlations among health states. In Lima city, the correlations are close to 1 when they are positive and close to −1 when negative. The districts with a fewer number of people have slightly lower correlations close to 0.9 and −0.9, respectively. It was shown in Ceferino et al. (2018) that the casualty severity covariance is evaluated by the sum of the average of all covariance realizations and the covariance of all mean realizations. In the case of Lima, the average of all covariance realizations is small compared with the covariance of the mean realizations. Thus the correlation is governed by the second term, namely, the covariance of the mean realizations. In addition, the mean realizations show a strong linear trend, thus causing high correlation of casualty severity. Though the correlations across health states are strong in this analysis, further evaluations are needed to identify the specific factors of the case study (e.g., large earthquake magnitude, extent of the geographic region of analysis, and vulnerable infrastructure) that drive such strong correlations and whether this trend is particular to the case study or if it can be generalized to other earthquake scenarios or other regions of analysis.

Correlation Across Multiple Districts

The model presented herein can also estimate the spatial correlations of casualty occurrence across several districts. This information is important for two reasons: (1) it provides an understanding on the dependencies of the casualty occurrence in close-distance districts and on how the degree of dependency drops off for more distant districts; and (2) it provides the basis for understanding joint casualty occurrences in multiple districts, which is key for joint hospital collaborative treatment of casualties across districts. These points will be further shown in the next subsection.

Figure 9 shows the estimated correlograms for different casualties calculated using Algorithm 2. For example, Figure 9a shows the correlogram for injuries with severity 3. The coordinates of each black dot represent the correlation between the number of casualties with severity 3 of two districts and the separation distance between the centroids of the

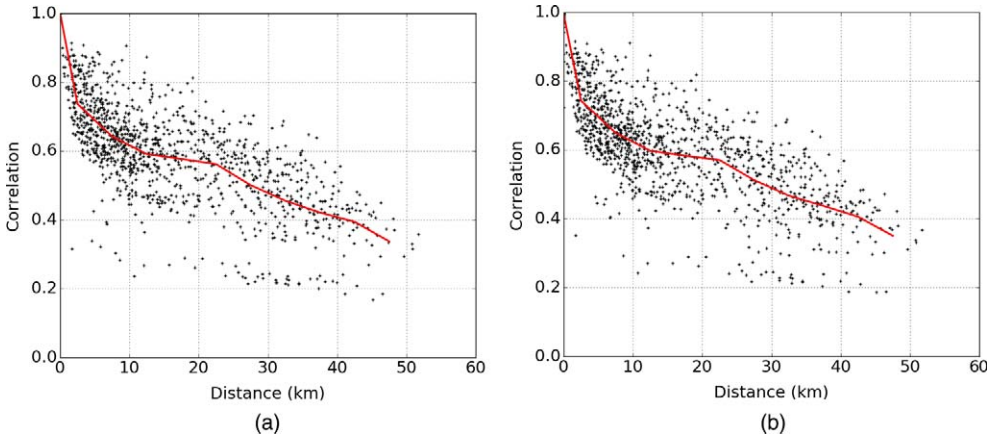

Figure 9. Correlation between the number of casualties in two districts as function of the distance between the districts: (a) Auto-correlogram for severity 3; and (b) cross-correlogram for severity 2 and severity 3.

districts. There are as many points as possible pairs of districts from the total set of 49 districts (1,225 dots). The red line is the average correlogram resulting from the black points. The correlogram shows that the correlation decays as a function of the separation distance. It starts at 1 for 0 km, and it decreases to 0.5 (on average) for 30 km of separation. This correlation decays to almost 0.35 at 50 km of separation. Figure 9b shows the cross-correlogram between casualties of severity 2 and 3. This measures the correlation between the number of casualties with severity 2 and 3 as a function of distance. It can be seen the cross-correlogram has as high values as the correlograms for severity 3. Analytically, the cross-correlogram at distance 0 km equals the correlation between severity 2 and 3. According to the plot, this value is very close to 1, which reflects the high correlations between different injury severities and fatalities (see Figure 8).

Noncollaborative versus Collaborative Hospital Response

Finally, another potentially important use of this casualty model is evaluating how responding to casualties with collaboration across different districts increases the likelihood of successfully treating people. The following example shows evidence that supports this hypothesis. First, the analysis focuses on casualties with severity 3 $(I_{hs_4,d})$ for five neighboring districts: El Agustino, La Victoria, Lima, Breña, and Rímac. It is assumed that the districts have medical capacity (C_d) to treat equal to $\mu - \sigma$ in each district d. This assumption is made to reflect the potential reduction in hospital capacity because of damage to the facility itself. The districts and corresponding capacities are reported in Table 3. Additionally, the marginal probability of meeting health care demands given these capacities are given in the third row of the table. It can be seen that these marginals are very similar in all districts and close to 0.42. These marginal responses indicate the probabilities of meeting the medical demands in the district jurisdiction according to the corresponding medical resources in each of the districts.

At a higher management level, that is, for an emergency planner in charge of multiple districts, the objective is that every district treats as many injured people as possible. If a

Table 3. Assumed capacity and corresponding marginal reliability in each district

Districts	El Agustino	La Victoria	Lima	Breña	Rímac
Capacity (C_d)	138	107	360	42	60
Marginal $(P[I_{hs_4,d} < C_d])$	0.42	0.42	0.42	0.42	0.43

noncollaborative hospital response is adopted across districts, each patient can only be treated within his or her jurisdiction. Figure 10a shows the joint probabilities of casualties with severity 3 in El Agustino and La Victoria districts and associated probability domain where this noncollaborative policy will be successful. The domain where both districts will meet the medical demands is shown in gray (i.e., the number of casualties is less than the corresponding district medical capacity in both districts); the other part of the domain is shown in red (i.e., the casualties were larger than corresponding district medical capacity in at least one district). The second column of Table 4 shows the probability of satisfying demands in both districts according to the noncollaborative policy. The probabilities of the effectiveness of this policy (i.e., meeting the demands in all districts) for multiple districts can be calculated using the same logic. The third, fourth, and fifth columns of Table 4 show the probabilities for meeting demands in three, four, and five districts, respectively. As it can be seen, when the number of communities increases, the probability of meeting the health demands in all districts consistently reduces.

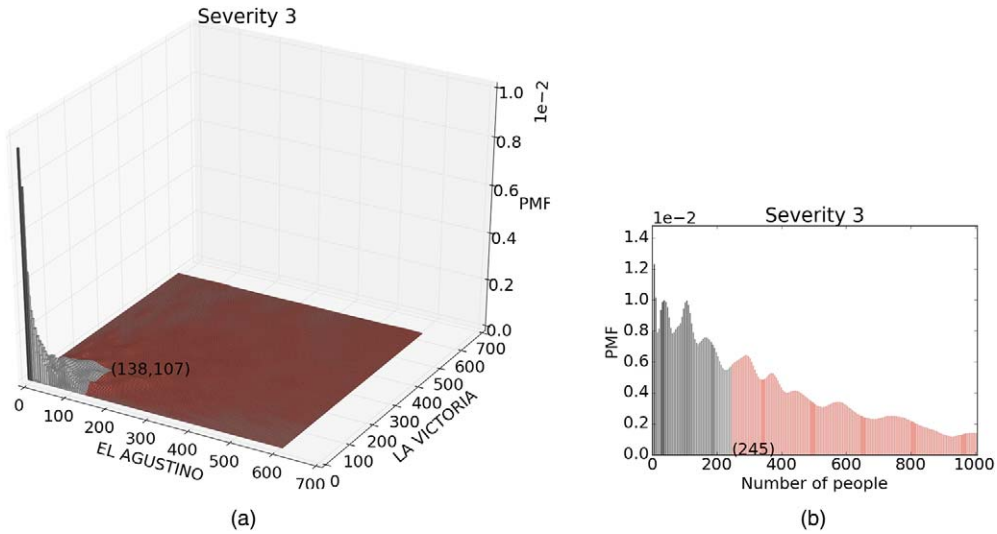

Figure 10. Hospital response to casualties with severity 3 in El Agustino and La Victoria districts: (a) Noncollaborative response; and (b) collaborative response. The probabilities masses have been binned in intervals of width 5 for visualization purposes.

Table 4. Noncollaborative versus collaborative response

	Joint individual response				Collaborative response			
Districts	$P[\cap_{d=1}^{n} I_{hs_3,d} < C_d]$				$P[\sum_{d=1}^{n} I_{hs_3,d} < \sum_{d=1}^{n} C_d]$			
El Agustino								
La Victoria	0.32				0.40			
Lima	–	0.29			–	0.40		
Breña	–	–	0.24		–	–	0.40	
Rímac	–	–	–	0.22	–	–		0.40

However, if a collaborative policy is implemented in which the hospital system treats injuries across different districts, then the probabilities of meeting the demands are higher compared with the noncollaborative policy. Under this policy, hospitals will treat patients from any other district, assuming that they have extra medical resources. For example, if El Agustino and La Victoria districts act together, then the total capacity of both will be the sum of both individual capacities. Similarly, the demands on the hospital system will be the sum of the demands on each of the districts. Figure 10b shows the distribution of the sum of casualties with severity 3 in El Agustino and La Victoria districts; the gray region represents the successful events that lead to treating all the casualties with severity 3 in both districts acting according to a collaborative policy. The red region, on the other hand, represents the events that exceeded the medical capacity of the hospital system. The probability of a successful response of the collaborative hospital system for the two-district case is reported in the sixth column of Table 4. Similarly, the probabilities for the three-, four- and five-district collaborative responses are shown in the seventh, eight, and ninth columns in Table 4. These results indicate that the likelihood of meeting the health demands after an earthquake can significantly increase when hospitals cooperate across different districts. In contrast to the noncollaborative policy, the probability of meeting the health care demands in multiple districts is not reduced. Therefore, when multiple communities are affected by an earthquake, the collaborative policy is more effective than the noncollaborative policy.

CONCLUSIONS AND RECOMMENDATIONS

This paper presented the application of the probabilistic casualty model proposed in Ceferino et al. (2018) to forecast the number of casualties and their severities in a region. In addition, this paper shows how such forecasts can provide useful information for earthquake risk mitigation policy makers and earthquake emergency planners. The model application was achieved through an earthquake scenario of Mw 8.8 occurring on the subduction zone off the coast of Peru and affecting Lima city. The data of the study include the Earthquake Event definition, the Soil Condition information, the Building Structural Typology, and the Building Occupancy Dynamics data. Additionally, the data requirements of the probabilistic modules' parameters are detailed, including the Ground Motion Intensity, the Building Damage, and the Population Health State modules.

This work shows the step-by-step procedure for implementing the two proposed algorithms for solving the casualty model: Algorithm 1 based on Monte Carlo and Algorithm 2

that combines Monte Carlo with the CLT. These procedures are used to estimate the mean values, uncertainties, and dependencies of multiseverity casualties by propagating the uncertainties and dependencies of ground motions, building damages, and building casualty occurrences.

The application shows the estimation of the joint probability distribution of casualties with multiple severities in Lima. Additionally, dependencies of casualties across different severities and different communities (spatial dependencies) were studied. It was shown that there is a positive correlation between casualty severities and a negative correlation between noninjured states and casualty states. The paper also showed four other useful model outcomes through the application. (1) Risk-informed demand-based hospital capacity targets: Hospital decision makers can target the 90th percentiles of casualties (or chose other percentiles) when making decisions on post earthquake hospital system target capacities. This information is unique, as existing methodologies (e.g., HAZUS) provide only mean number of multiseverity casualties. (2) Identification of urban districts and structural typologies with the highest casualty rates in a region: These results can be used to inform policy making into the strengthening of the most unsafe structural typologies in the region and focus on the most vulnerable districts. (3) Casualty forecasting in regions with limited earthquake casualty data: The proposed model provides multiseverity casualty estimates accounting for current population growth and infrastructure vulnerability. This approach provides an advantage over country-specific, empirical methods, as they may underestimate fatalities for regions where casualty data are scarce and not recent. (4) Testing effectiveness of hospital system collaborative policies: The model can be used to investigate various hospital system collaborative decisions. This paper shows that hospitals that collaborate across multiple districts have a greater probability of treating injuries than hospitals that do not collaborate, thus potentially leading to a higher state of resilience for the city. This key result should encourage hospital systems to enforce collaboration across different districts and to enhance their capacity for communication, coordination, and transportation of patients.

ACKNOWLEDGMENTS

This research was partially supported by NSF EAGER Grant Number CMMI-1645335 and the Shah Family Fellowship through the Department of Civil and Environmental Engineering at Stanford University. The authors are grateful for their generous support. In addition, the authors thank Vitor Silva, Mabe Villar, and Catalina Yepes from the Global Earthquake Model (GEM) for providing data on the building exposure in Lima city and their valuable feedback and comments on the preliminary results of this paper; Jorge Morales and Miguel Estrada from the National University of Engineering in Peru for providing data on the Soil Condition information in the city and their expertise in spatial processing of the building exposure data; and Maryia Markhvida from Stanford University for processing and sharing her expertise on the correlation of regional ground motions. The authors also appreciate the constructive comments and suggestions of the EERI reviewers of the paper.

APPENDIX

Please refer to the online version of this paper to access the supplementary material provided in the Appendix.

REFERENCES

Aguilar, Z., Lazares, F., Alarcón, S., Quispe, S., Uriarte, R., and Calderón, D., 2013. Actualización de la Microzonificación Sísmica de la cuidad de Lima, in *The International Symposium for CISMID 25th Anniversary* 17–18 August, 2012, Lima, Peru.

Allen, T. I., and Wald, D. J., 2007. *Topographic Slope as a Proxy for Seismic Site-Conditions (V_{S30}) and Amplification Around the Globe. Tech. Rep. 2007-1357*, United States Geological Survey, Reston, VA.

Beck, S. L., and Nishenko, S. P., 1990. Variations in the mode of great earthquake rupture along the central Peru subduction zone, *Geophysical Research Letters* **17**, 1969–1972.

Ceferino, L., Kiremidjian, A. S., and Deierlein, G. G., 2018. Probabilistic model for regional multi-severity casualty estimation due to bilding damage following an earthquake, *Special Collection of ASCE-ASME Journal of Risk and Uncertainty in Engineering Systems: Part A: Civil Engineering*. In press.

Dorbath, L., Cisternas, A., and Dorbath, C., 1990. Assessment of the size of large and great historical earthquakes in Peru, *Bulletin of the Seismological Society of America* **80**, 551–576.

Federal Emergency Management Agency (FEMA), 2015. *Multi-Hazard Loss Estimation Methodology: Earthquake Model, Hazus–MH 2.1: Technical Manual* Washington, D.C., available at http://www.fema.gov/media-library-data/20130726-1820-25045-6286/hzmh2_1_eq_tm.pdf (last accessed 1 August 2017).

Global Earthquake Model (GEM) Secretariat, 2015. *On the South America Risk Assessment (SARA) Final Report 2015, Version 1.0. Tech. Rep.*, GEM Foundation, Pavia, Italy.

Goda, K., and Atkinson, G. M., 2009. Probabilistic characterization of spatially correlated response spectra for earthquakes in Japan, *Bulletin of the Seismological Society of America* **99**, 3003–3020.

Goda, K., and Hong, H. P., 2008. Spatial correlation of peak ground motions and response spectra, *Bulletin of the Seismological Society of America* **98**, 354–365.

Goncharov, S., and Frolova, N., 2011. Chapter 10: Casualty estimation due to earthquakes: injury structure and dynamics, *Human Casualties in Earthquakes: Progress in Modelling and Mitigation* (R. Spence, E. So, C. Scawthorn, eds.), Springer, New York, NY, 141–152.

Jaiswal, K., and Wald, D., 2010. An empirical model for global earthquake fatality estimation, *Earthquake Spectra* **26**, 1017–1037.

Jaiswal, K., Wald, D. J., and Hearne, M. G., 2009. *Estimating Casualties for Large Earthquakes Worldwide Using an Empirical Approach, Tech. Rep. 2009–1136*, U.S. Geological Survey (USGS) Reston, VA.

Johnston, D., Standring, S., Ronan, K., Lindell, M., Wilson, T., Cousins, J., Aldridge, E., Ardagh, M. W., Deely, J. M., Jensen, S., Kirsch, T., and Bissell, R., 2014. The 2010/2011 Canterbury earthquakes: context and cause of injury, *Natural Hazards* **73**, 627–637.

Lallemant, D., Burton, H., Ceferino, L., Bullock, Z., and Kiremidjian, A., 2017. A framework and case study for earthquake vulnerability assessment of incrementally expanding buildings, *Earthquake Spectra* **33**, 1369–1384.

Markhvida, M., Ceferino, L., and Baker, J. W., 2018. Modeling spatially correlated spectral accelerations at multiple periods using principal component analysis and geostatistics, *Earthquake Engineering & Structural Dynamics* **47**, 1107–1123.

Ministerio de Vivienda, 2016. Norma Técnica E.030 Diseño Sismorresistente.

Noh, H. Y., Kiremidjian, A., Ceferino, L., and So, E., 2017. Bayesian updating of earthquake vulnerability functions with application to mortality rates, *Earthquake Spectra* **33**, 1173–1189.

Oak Ridge National Laboratory, 2013. LandScan Global Population Database, available at https://purl.stanford.edu/dd452vk1873 (last accessed 1 August 2017).

Silva, V., Crowley, H., Pagani, M., Monelli, D., and Pinho, R., 2014. Development of the OpenQuake engine, the Global Earthquake Model's open-source software for seismic risk assessment, *Natural Hazards* **72**, 1409–1427.

U.S. Geological Survey (USGS), 2015. *Earthquakes with 1,000 or More Deaths 1900–2014, Tech. Rep*., USGS, Reston, VA.

Villar-Vega, M., Silva, V., Crowley, H., Yepes, C., Tarque, N., Acevedo, A. B., Hube, M. A., Gustavo, C. D., and Santa María, H., 2017. Development of a fragility model for the residential building stock in South America, *Earthquake Spectra* **33**, 581–604.

Walker, C., 2008. *Shaky Colonialism: The 1746 Earthquake-Tsunami in Lima, Peru, and Its Long Aftermath*, Duke University Press, Durham, NC.

Wells, D. L., and Coppersmith, K. J., 1994. New empirical relationships among magnitude, rupture length, rupture width, rupture area, and surface displacement, *Bulletin of the Seismological Society of America* **84**, 974–1002.

Yepes-Estrada, C., Silva, V., Valcárcel, J., Acevedo, A. B., Tarque, N., Hube, M. A., Coronel, G., and Santa María, H., 2017. Modeling the residential building inventory in South America for seismic risk assessment, *Earthquake Spectra* **33**, 299–322.

Zhao, J. X., Zhang, J., Asano, A., Ohno, Y., Oouchi, T., Takahashi, T., Ogawa, H., Irikura, K., Thio, H. K., Somerville, P. G., Fukushima, Y., and Fukushima, Y., 2006. Attenuation relations of strong ground motion in Japan using site classification based on predominant period, *Bulletin of the Seismological Society of America* **96**, 898–913.

(Received 6 August 2017; accepted 23 April 2018)